Aerospace Science and Technology 91 (2019) 301–309

Contents lists available at ScienceDirect

Aerospace Science and Technology

www.elsevier.com/locate/aescte

Assessment of a one-dimensional finite element charring ablation material response model for phenolic-impregnated carbon ablator

Yeqing Wang [a,*], Timothy K. Risch [b], Joseph H. Koo [c]

[a] Department of Aerospace Engineering, Mississippi State University, Mississippi State, MS 39762, USA
[b] NASA Armstrong Flight Research Center, Edwards Air Force Base, CA 93523, USA
[c] Department of Mechanical Engineering, The University of Texas at Austin, Austin, TX 78739, USA

ARTICLE INFO

Article history:
Received 26 February 2019
Received in revised form 28 April 2019
Accepted 13 May 2019
Available online 17 May 2019

Keywords:
Hypersonic re-entry
Charring ablation
Phenolic-impregnated carbon ablator
Pyrolysis
Oxy-acetylene torch
Finite element analysis (FEA)

ABSTRACT

In this study, mathematical formulations to model charring ablation problems were numerically implemented using finite element analysis (FEA) with ABAQUS, which account for the material decomposition and progressive surface removal in the heat conduction and the surface energy balance equations. FEA was performed for a one-dimensional model to predict the temperature and ablation histories of a phenolic-impregnated carbon ablator sample (i.e., a common heat shield material for hypersonic vehicles and spacecraft) subjected to oxy-acetylene torch flame (i.e., 0.8 SLPM acetylene gas to 2.7 SLPM oxygen gas). The recovery enthalpy and convective heat transfer coefficient for the ablation model were calculated based on gas compositions and two assumed surface conditions (i.e., equilibrium and frozen). Simulations using the calculated recovery enthalpy and convective heat transfer coefficient resulted in a recession rate of 6.38 times (equilibrium) and 14.08 times (frozen) higher than the experimental data, despite fair agreement of the surface temperature. In addition, the effect of the heat transfer coefficient was investigated through a steady-state ablation analysis. The results of the analysis indicate that there is not one single value for the heat transfer coefficient that would allow the prediction to match both measured recession rate and surface temperature. Possible reasons for such an inconsistency are provided and discussed.

Acronyms

ACE	Aerotherm Chemical Equilibrium
ALE	Arbitrary Lagrangian-Eulerian
CEA	Chemical Equilibrium with Applications
CHAR	CHarring Ablator Response
CMA	Charring Material Ablation
FEA	Finite Element Analysis
FIAT	Fully Implicit Ablation and Thermal
HERO	Heat Transfer and Erosion Analysis
PICA	Phenolic Impregnated Carbon Ablator
TACOT	Theoretical Ablative Composite for Open Testing

1. Introduction

One of the significant challenges for hypersonic vehicles and spacecraft is the design of effective thermal protection systems (TPS) that aims to prevent the extremely high aerodynamic heating from damaging the internal structural components during the hypersonic flight. For typical low earth orbit re-entry vehicles, the maximum speed can reach nearly Mach 25 and the maximum surface temperature can reach nearly 3000 K [1]. Under such an extreme condition, conventional load-bearing light-weight structural materials such as aluminum alloys are unable to survive due to their low maximum service temperature. To withstand the extremely high temperature, a layer of ablative materials (i.e., the heat shield), such as the phenolic-impregnated carbon ablator (PICA), is bonded to the blunt body of the spacecraft or the airframes of the hypersonic vehicle [2,3]. During the hypersonic re-entry, the heat shield absorbs thermal energy from the external flow and dissipates the thermal energy by progressively removing the ablative material through vaporization, oxidation, etc., and, thus, serves to protect the internal structural components.

In particular, charring ablation is a result of surface chemical reactions that progressively consumes the char layer of the ablative material, where the char layer is formed after the material is completely decomposed under elevated temperatures [4]. The energy balance at the material surface ascribes to complex convective and radiative heat exchanges between the external flow and the material, as well as the heat loss due to the release of pyrolysis gas and progressive surface material removal. Meanwhile,

* Corresponding author.
E-mail address: yw253@msstate.edu (Y. Wang).

https://doi.org/10.1016/j.ast.2019.05.039
1270-9638/

Nomenclature

Roman & Greek symbols

B'	normalized recession rate	$\dot{m}_c/\rho_e U_e C_H$
C_p	specific heat	J/(kg-K)
C_H	"blown" Stanton number	
C_{HO}	"unblown" Stanton number	
E	activation energy	J/mol
h	enthalpy	J/kg
$\overline{h}$	mass weighted averages of the material enthalpy	J/kg
$\dot{m}_g$	pyrolysis gas mass flux	kg/(m^2-s)
k	thermal conductivity	W/(m-K)
p	pressure of pyrolysis gas	atm
q	heat flux	W/m^2
R	universal gas constant	8.314 J/(mol-K)
$\dot{s}$	surface recession rate	m/s
T	temperature	K
t	time	s
y	in-depth direction coordinate	m
α	decomposing rate coefficient	1/s
ρ	density	kg/m^3
σ	Stefan-Boltzmann constant	W/(m^2-s-K^4)
ε	emissivity coefficient	
ψ	reaction order	
$\rho_e U_e C_H$	heat transfer coefficient	kg/(m^2-s)

Subscripts

c	char
e	freestream
g	pyrolysis gas
r	recovery
s	surface
v	virgin
w	wall
∞	background condition

the in-depth heat conduction governing equation also needs to account for those various effects. Here, the surface energy balance and the in-depth heat conduction equations form the basic mathematical formulation for modeling the charring ablation problems. To implement such a formulation, various numerical tools have been developed to date. One of the first successful tools is the Charring Material Ablation (CMA) program developed by the Aerotherm Corporation in the late 1960's [5] and still in use today. Later, a Fully Implicit Ablation and Thermal (FIAT) analysis tool for modeling charring ablation was developed by NASA Ames based on identical fundamental physical assumptions to those used in CMA [6]. Predictions from CMA and FIAT are often used as baselines for code-to-code verifications. The common feature of CMA and FIAT is that they are limited to one-dimensional (1-D) geometries (or configurations), and, thus, are unable to fully capture the effects of the complex geometric features on the thermal and ablative response. Subsequently, FIAT was extended to two and three-dimensional (2-D and 3-D) geometries through the development of TITAN [7] and 3dFIAT [8], respectively. In addition, another common feature of the aforementioned analysis tools is that they are based on finite difference or finite volume methods. For example, the CMA was developed based on a finite difference method and the FIAT was developed based on a finite volume method. Other reported ablation analysis tools were also developed based on these two numerical methods [9–20]. For example, a 1-D pyrolysis layer model was developed based on a central difference numerical scheme and employed to investigate the nonlinear thermal behavior of the AVCOAT composites [15] and other novel designs of homogeneous and non-homogeneous charring composites [16]. Moreover, the mathematical equations of a coupled thermal/fluid/chemical/ablation model were discretized using central-difference and upwind numerical schemes. Such a coupled model was implemented through FORTRAN and MATLAB codes and validated through comparisons with experimental data [17]. Other numerical models developed by the finite difference method have also been used to predict, for example, the surface ablation behavior of SiFRP composites under a steady state ablation condition [18] and the thermal and chemical non-equilibrium of ablation and pyrolysis of a carbon-phenolic ablator [19]. Furthermore, a chemical equilibrium heat and mass transport model for porous ablators was developed based on the volume-averaged finite-volume method, which was implemented in the Porous material Analysis Toolbox based on OpenFOAM (PATO) [20]. This model was applied to the detailed analysis of the boundary layer and pyrolysis gas flows within a porous carbon-phenolic ablator featuring the arc-jet testing environment.

Recently, finite element method has received more and more attention due to the improved computational capabilities, flexibility, and enhanced applicability especially to complex geometries, as opposed to the finite difference (or volume) method [4,21–23]. A few numerical tools for modeling charring ablation based on finite element method have been recently developed, such as the CHarring Ablator Response (CHAR) code [24] and the Heat Transfer and Erosion Analysis (HERO) program [25]. However, these tools are custom written and not as flexible and versatile as general purpose FEA programs. The commercial, general-purpose finite element analysis (FEA) programs such as ABAQUS, provide an alternative solution for modeling charring ablation problems. When compared to the custom-written programs, the commercial, general-purpose FEA programs provide enhanced capabilities in terms of usability, pre and post-processing, mesh generation, flexibility, as well as interfaces that allow users to couple the structural analysis with computational fluid dynamics (CFD). However, the built-in heat transfer analysis steps provided by these programs are often restricted to modeling conventional heat transfer problems without considering the effects of material decomposition or surface material removal and, thus, are unable to model charring ablation problems. To enable the capability of modeling charring ablation problems using these programs, additional user subroutines must be developed to accommodate those effects through accurate modifications of the built-in heat conduction governing equation and surface energy balance yielded boundary conditions.

In this paper, FEA was performed for a 1-D charring ablation model using ABAQUS through the development of multiple user subroutines along with the arbitrary Lagrangian-Eulerian (ALE) adaptive meshing algorithm. The subroutines enable users to implement the mathematical formulation of the charring ablation problem and track the moving boundary condition due to the progressive surface material removal, while the ALE adaptive meshing algorithm allows the computational domain to be automatically remeshed after the material surface is progressively removed from the domain. The numerical procedure solves sequentially the temperature and the density change (i.e., the temperature is solved first and then used to calculate the density change afterwards). The proposed model has been successfully verified by comparing the predictions of the temperature and ablation histories with those obtained using the well-validated charring code, FIAT, in the authors' early work [26]. In this paper, we attempt to validate the

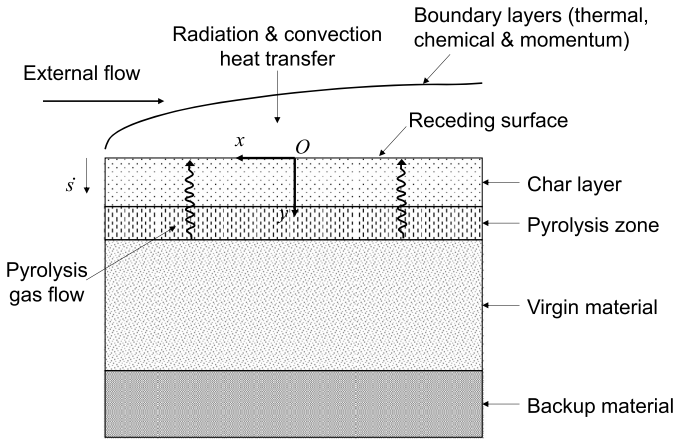

Fig. 1. Illustration of the physical process during ablation.

proposed model by comparing the simulation results with the experimental data reported by Refs. [27,28].

The remainder of the paper is organized as follows. In Section 2, the physical process of the ablative material during ablation is briefly described. Additionally, the mathematical formulations for modeling the charring ablation problems are provided. In Section 3, the numerical implementation for a 1-D charring ablation model using FEA with ABAQUS is introduced, where the implementation includes multiple user subroutines along with the ALE adaptive meshing algorithm. In Section 4, the convective heat transfer coefficient and the recovery enthalpy are calculated and used to perform the numerical simulations. The simulation results, including the averaged surface temperature and the recession rate, are compared to the experimental data for model validation. In addition, a steady-state ablation analysis is provided to investigate the effect of the convective heat transfer coefficient on the averaged surface temperature and the recession rate. Concluding remarks are given in Section 5.

2. Physical description of the ablation problem and fundamental equations

2.1. Physical description of the ablation problem

Ablative materials, such as PICA, are commonly used as the outer layer of the heat shield for atmospheric re-entry vehicles. Such an ablative layer is typically followed by a non-ablative structural backup material (see Fig. 1). During entry, the surface temperature of the ablative material increases under complex convective or radiative heating. As the temperature increases, the material undergoes various surface chemical reactions (e.g., oxidation, nitridation, and vaporization) which leads to the surface material removal. In addition, the in-depth conduction of thermal energy leads to the decomposition of the material and the liberation of pyrolysis gas. The induced pyrolysis gas travels upward through the pores of the material and contributes to the surface energy balance. Fig. 1 shows the three regimes that the ablative material experiences during the atmospheric re-entry, where the virgin material refers to the ablative material before it starts to decompose, the pyrolysis zone refers to the region where the ablative material starts to decompose but is not fully decomposed, and the char layer refers to the layer where the ablative material has fully decomposed.

2.2. Fundamental equations

The fundamental equations for the charring ablation problem, including the in-depth heat condition equation and the surface energy balance equation can be found in many open literature [4,8,14,29–34]. In the below two sections, we provide a brief review of these equations.

2.2.1. Governing equation

The in-depth heat conduction equation that considers the decomposition of material and surface material removal for a 1-D ablation problem in a coordinate x fixed in space is written as

$$\rho C_p \left.\frac{\partial T}{\partial t}\right|_y = \frac{\partial}{\partial y}\left(k\frac{\partial T}{\partial y}\right) + \left(h_g - \bar{h}\right)\left.\frac{\partial \rho}{\partial t}\right|_y + \dot{s}\rho C_p \frac{\partial T}{\partial y} + \dot{m}_g \frac{\partial h_g}{\partial y}, \tag{1}$$

where ρ, C_p, and k are the density, specific heat, and thermal conductivity of the material, respectively, h_g is the pyrolysis gas enthalpy, $\bar{h}$ is the mass weighted averages of the material enthalpy, $\dot{s}$ is the speed of the local coordinate movement due to the continuous surface recession (see detailed discussion in Section 2.2.2), $\dot{m}_g$ is the pyrolysis gas mass flux, y is the in-depth direction coordinate, and T is the temperature.

In Eq. (1), the local specific heat and thermal conductivity of the material are temperature-dependent, and can be calculated using the rule of mixture providing the temperature-dependent properties for the virgin material and char

$$k = \delta k_v + (1-\delta)\, k_c, \tag{2}$$

$$C_p = \delta C_{p,v} + (1-\delta)\, C_{p,c}, \tag{3}$$

where subscripts v and c denote the virgin material and char, respectively, and δ is the volume fraction of the undecomposed material, expressed by

$$\delta = \frac{\rho_v}{\rho_v - \rho_c}\left(1 - \frac{\rho_c}{\rho}\right). \tag{4}$$

Note that the ablative material is a composite material that consists of two types of resin filler components and one reinforcement component, the density of the overall composite material is given by

$$\rho = \Gamma\left(\rho_A + \rho_B\right) + (1-\Gamma)\,\rho_C, \tag{5}$$

where subscripts A and B denote the two resin filler components, subscript C denotes the reinforcement component, and Γ is the volume fraction of resin. For each component, the rate of density variation due to the decomposition follows an Arrhenius equation

$$\frac{\partial \rho_i}{\partial t} = -\alpha_i \exp\left(-\frac{E_i}{RT}\right)\rho_{v,i}\left(\frac{\rho_i - \rho_{c,i}}{\rho_{v,i}}\right)^{\psi_i}, \tag{6}$$

where subscript $i = A$, B, and C, α is the decomposing rate coefficient, R is the universal gas constant, ψ is the reaction order.

In addition, the mass weighted averages of the material enthalpy (i.e., $\bar{h}$ in Eq. (1)), is written as

$$\bar{h} = \frac{\rho_v h_v - \rho_c h_c}{\rho_v - \rho_c}, \tag{7}$$

where h is the enthalpy of the ablative material.

The pyrolysis gas enthalpy is both temperature and pressure-dependent (i.e., h_g in Eq. (1), and $h_g = h_g(p, T)$, p being the pressure of the pyrolysis gas) which is often determined through equilibrium thermochemistry analysis. Finally, the pyrolysis gas mass flux (i.e., $\dot{m}_g$ in Eq. (1)), at any location, y, in the case of a 1-D ablation problem, can be calculated using

$$\dot{m}_g = -\int_0^y \frac{\partial \rho}{\partial t} dy. \tag{8}$$

Note that for charring ablation problems with multiple dimensions, the divergence of the gas flow is calculated from the local reaction rate in all directions [4]:

$$\nabla \cdot \dot{m}_g = \frac{\partial \rho}{\partial t}. \tag{9}$$

Using Eq. (9), the pressure can be determined from Darcy's law or some other relationship between pressure and mass flow rate or velocity.

2.2.2. Surface energy balance equation yielded boundary conditions

The surface energy balance equation that accounts for the surface material removal for the material during ablation is written as

$$-k\frac{dT}{dy} = \rho_e U_e C_H \cdot (h_r - h_w) + \rho_e U_e C_H \cdot \left(B'_c h_c + B'_g h_g - B' h_w\right) - \sigma \varepsilon \left(T_w^4 - T_\infty^4\right), \tag{10}$$

where $\rho_e U_e C_H$ is the convective heat transfer coefficient (ρ and U being the density and velocity of the flow, subscript e denoting the local conditions at the edge of the boundary layer, and C_H being the Stanton number). In addition, subscript r refers to the recovery conditions at the wall for zero heat transfer (i.e., h_r is the recovery enthalpy), subscript w refers to the conditions at the wall (i.e., the material surface), subscript ∞ refers to the ambient environment, σ is the Stefan-Boltzmann constant, and ε is the emissivity. Here, the recovery enthalpy, h_r, is calculated by using a rule of mixture with the mass fraction composition of the gas mixture (see Table 1 in Section 4.2), the char enthalpy of the PICA material, h_c, is taken from the TACOT material system (see Section 4.3), and the wall enthalpy, h_w, is calculated using the NASA Aerotherm Chemical Equilibrium (ACE) program with the thermodynamic data supplied from the NASA Chemical Equilibrium with Applications (CEA) database [35].

Moreover, B' in Eq. (10) is the total mass loss rate, defined by

$$B' = B'_c + B'_g, \tag{11}$$

with B'_g being the non-dimensional mass loss rate due to the release of the pyrolysis gas, and B'_c being the non-dimensional mass loss rate due to the char consumption. Here, B'_g can be calculated using

$$B'_g = \frac{\dot{m}_g}{\rho_e U_e C_H}, \tag{12}$$

where $\dot{m}_g$ is the mass flux of the pyrolysis gas. The non-dimensional mass loss rate due to the char consumption, B'_c and the enthalpy of the gas phase just above the surface, h_w are both dependent on the wall temperature, T_w, the pressure, p, and the non-dimensional mass loss rate due to the release of the pyrolysis gas, B'_g. The dependencies of the B'_c and h_w on the T_w, p, and B'_g are also known as the surface thermochemistry relations which can be calculated using a third party program, i.e., the NASA ACE program with the thermodynamic data supplied from the NASA CEA database [35]. With the obtained surface thermochemistry relations, the B'_c and h_w are calculated by providing the T_w, p, and B'_g at each time increment during the computation. Note that in this study, the pressure, p, is assumed to hold at 1 atm throughout this study to simulate the ablation test in the ambient environment [36]. After B'_c is obtained, the mass loss rate due to charring, $\dot{m}_c$, is calculated using

$$\dot{m}_c = B'_c \cdot \rho_e U_e C_H. \tag{13}$$

Here, the Stanton number is reduced by blowing from the surface and corrected using an expression derived from the film theory [37]

$$\frac{C_H}{C_{HO}} = \frac{\ln\left(1 + 2\lambda B'\right)}{2\lambda B'}, \tag{14}$$

where C_H is the corrected or "blown" Stanton number and C_{HO} is the unblown values.

Finally, the speed of the local coordinate movement, $\dot{s}$ (i.e., the speed of the surface recession) can be obtained using

$$\dot{s} = \frac{\dot{m}_c}{\rho_s}, \tag{15}$$

where ρ_s is the local density at the material surface. Notice that Eq. (15) contributes to the coupling between the in-depth heat conduction and the material surface removal (see $\dot{s}$ in Eq. (1)).

3. Numerical implementation with finite element analysis in ABAQUS

The built-in heat transfer analysis step provided in ABAQUS is often used for modeling general heat conduction problems without considering the material decomposition or surface material removal and, thus, is not suitable for modeling the charring ablation problems with a formulation described in Section 2.2. In addition, ABAQUS assumes that the driving force of the convective heat exchange for a heat transfer analysis is the temperature difference (between the boundary layer and the material surface) and only allows the user to define the convective boundary condition as a function of the temperature difference in the ABAQUS input interface. However, for charring ablation problems, it is more useful to deal in enthalpy than temperature in defining a heat transfer coefficient (see Eq. (10)). A convective boundary condition with enthalpy cannot be directly defined in the ABAQUS input interface. To overcome these limitations, additional user subroutines must be developed to enable ABAQUS with the capability of implementing the charring ablation formulation.

To model charring ablation problems, the ABAQUS coupled temperature-displacement step is used. In addition, multiple subroutines are developed to modify the built-in heat conduction and surface energy balance equations (see Section 2.2.2). In particular, a FILM subroutine [38], which is normally used to define the sink temperatures as functions of position, time, temperature, etc., is developed to obtain the material surface temperature (T_w) at each time increment. Meanwhile, a USDFLD subroutine [38] is developed to update the material properties (e.g., thermal conductivity, specific heat, and enthalpy), rate of density change, mass flux, and B'_g corresponding to the instant temperature field after each time increment. Note that the integral in Eq. (8) (i.e., the pyrolysis gas mass flux) is computed using the Simpson's rule. Then, T_w (from the FILM subroutine) and B'_g (from the USDFLD subroutine) are passed to a DFLUX subroutine [38] to obtain the instant wall enthalpy (i.e., $h_w = h_w(T_w, p, B'_g)$) and the mass loss rates (i.e., $B'_c = B'_c(T_w, p, B'_g)$ and $B' = B'_c + B'_g$) based on surface thermochemistry relations. The obtained h_w, B'_c, and B' are plugged into Eq. (10) and, thus, the surface energy balance yielded boundary condition is determined in the DFLUX subroutine. Furthermore, a UMATHT subroutine [38] is developed to define the heat conduction (Eq. (1)) that accounts for the material decomposition (Eqs. (6) and (8)) and the surface material removal (Eq. (15)). The

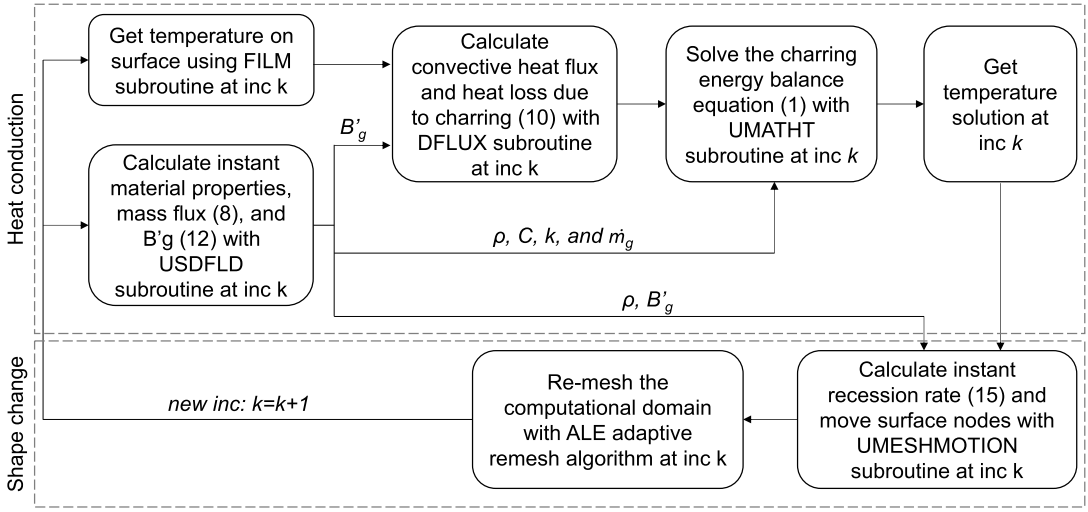

Fig. 2. Flowchart of the FEA implementation in ABAQUS with multiple subroutines for modeling charring ablation problems.

instant material properties obtained from the USDFLD subroutine are passed to the UMATHT subroutine to obtain the internal energy variation and the heat flux vector. Then, the temperature solution at each time increment is obtained by solving the governing equation (Eq. (1)) with the surface boundary condition (Eq. (10)). Next, the temperature solution along with the instant density change and B'_g obtained from the USDFLD subroutine are transferred to the UMESHMOTION subroutine [38] to calculate the instant recession rate (Eq. (15)) and the ablation depth. With the calculated instant ablation depth, the UMESHMOTION subroutine moves the surface nodes to their new locations. After that, the entire computational domain is re-meshed with the ALE adaptive remesh algorithm and the re-meshed domain is used to calculate the temperature solution for the next time increment. In other words, the temperature is not calculated before the domain is re-meshed, only the temperature values associated with the current re-meshed domain is calculated at each time increment. Therefore, the material properties including the enthalpy updated using the temperature values associated with the current re-meshed domain are real values. This procedure repeats until the last time increment, therefore enabling the coupling between the heat conduction considering material decomposition and the progressive surface material removal. It is worth stressing that the model solves sequentially the temperature and the density change. In addition, the data transfer between the different user subroutines is achieved using the common blocks provided by FORTRAN. The flowchart of the FEA implementation in ABAQUS is provided in Fig. 2. Note that a prior code-to-code verification has been performed for the proposed model against FIAT in the authors' early work [26]. It is also interesting to note that the proposed model and ABAQUS subroutines can also be modified and extended to study the lightning strike and laser ablations of carbon fiber reinforced polymer matrix composite materials [39–41].

4. Model assessment

4.1. Description of experimental test

The experimental data for model assessment is the ablation test data for PICA samples reported by Dr. Joseph Koo's Research Group at the University of Texas at Austin [27,28]. In the ablation test, four type-K thermocouples (TCs) were embedded at graduated depths within the PICA samples that allow for in-situ temperature history measurements. The locations of the TCs are shown in Fig. 3. The PICA samples were clamped and exposed to a heat flux

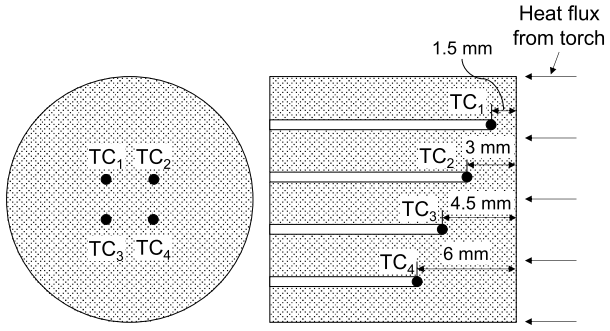

Fig. 3. Locations of four thermocouples that are embedded in the PICA samples for the oxy-acetylene torch ablation test, left: bottom view, right: cross-section view.

of 1×10^7 W/m^2 which was produced via an oxy-acetylene torch. The heat flux was measured with a Gardon gauge. The fuel ratio of the torch flame mixture is 1:3.375 by mole (i.e., 0.8 SLPM acetylene gas to 2.7 SLPM oxygen gas). The temperature history at the receding surface of the PICA samples was recorded using a 2-color infrared (IR) pyrometer, while the in-depth temperature histories were recorded using the four TCs. Meanwhile, as the material surface recedes during ablation, the TCs expose and break in succession, providing a series of break times and depths that allow to calculate the recession rate. The experimental data for temperature and ablation histories are compared with the numerical predictions in Section 4.4.

4.2. Estimation of the convective heat transfer coefficient and recovery enthalpy

To perform the model assessment, the convective heat transfer coefficient and the recovery enthalpy need to be determined to replicate the surface conditions on the PICA sample due to the oxy-acetylene torch flame. However, obtaining these parameters is a challenging task which often requires separate surface chemical reaction dynamics experimental tests. Such tests were not reported and no available parameters can readily be used in the ablation model. Langston et al. [27] attempted to calculate the two parameters using the Chemical Equilibrium with Transport Properties program (CET) [42] based on (i) the Fay-Riddell equation for stagnation point heat transfer [43] and (ii) the Victor's model [44]. However, their calculation led to a high recovery enthalpy and an incredibly low convective heat transfer coefficient (exact val-

Table 1
The mass fraction and the heat of formation of the oxy-acetylene mixture [45].

	Molecular Weight	Mole Composition	Mole Fraction	Mass Fraction	Compound	Mixture
					Heat of Formation	Heat of Formation
Unit	g/mol	–	–	–	kJ/g	kJ/g
Acetylene	26.03728	0.8	0.228571	0.19426	8.71366	1.693
Oxygen	31.9988	2.7	0.771429	0.80574	0	0
Total		3.5	1	1		1.693

Table 2
Calculated heat transfer coefficients for equilibrium and frozen conditions at the wall.

Heat flux at wall	Recovery enthalpy	Frozen		Equilibrium	
		Wall enthalpy	Heat transfer coefficient	Wall enthalpy	Heat transfer coefficient
W/m^2	J/kg	J/kg	$kg/(m^2\text{-s})$	J/kg	$kg/(m^2\text{-s})$
1×10^7	1692715	−2627506	2.314697	−7673014	1.067723

ues were not reported). Using those unrealistic parameters, the predicted surface temperature is 2000 K lower than the experimental data and the predicted total ablation depth is only 1.3% of the experimental data. Here, we remark that the analysis using the Fay-Riddell equation will not necessarily be accurate because the expression is derived for air, not for oxy-acetylene. In this study, we present an alternative approach to estimate those parameters.

For the convective heat transfer, the heat flux q is equal to the heat transfer coefficient $\rho_e U_e C_H$ multiplied by the difference in enthalpy between the freestream h_r (i.e., the recovery enthalpy) and the wall h_w:

$$q = \rho_e U_e C_H \left(h_r - h_w\right). \tag{16}$$

Then, the heat transfer coefficient therefore can be calculated by:

$$\rho_e U_e C_H = \frac{q}{(h_r - h_w)}. \tag{17}$$

To obtain the heat transfer coefficient using Eq. (17), first we need to compute the recovery enthalpy h_r. In order to do this, the mass fraction composition of the oxy-acetylene mixture needs to be determined. The volumetric (or mole) ratio of the acetylene (C_2H_2) to oxygen (O_2) is given as 0.8 to 2.7 (see Section 4.1), which gives a mass fraction of 19.4% acetylene to 80.6% oxygen, as shown in Table 1.

The heat of formation of acetylene and oxygen is 8.7137 kJ/g and 0, respectively. By taking into account the mass fraction, the heat of formation of the mixture (i.e., recovery enthalpy) is therefore 1.693 kJ/g.

The adiabatic flame temperature is calculated using the NASA ACE [46] with thermodynamic data supplied from the NASA CEA database [47]. The calculated temperature is 3287 K.

The next step to calculate the heat transfer coefficient is to determine the wall enthalpy h_w in Eq. (17). To do that, we considered two cases where the surface is composed of only acetylene and oxygen. The first case assumes equilibrium combustion of acetylene oxygen at the wall temperature (assumed to be 300 K) with only H_2O, CO_2, and CO species at the wall. The calculated enthalpy in this case using the ACE program is −2627.51 J/g. The second case assumes that the freestream composition is frozen at the wall in which case the calculated enthalpy is −7673.01 J/g. Here, it is worth mentioning that the calculated wall enthalpies under these two cases are for oxy-acetylene only and used to match the calibration. In addition, since the surface conditions are only composed of acetylene oxygen, there is no ablation under the two cases we considered. In other words, no pyrolyzing B'_g or charring B'_c is considered under those two cases. In reality, the actual wall enthalpy is in between these two values. However, given that the pressure is 1 atm, the actual wall enthalpy is likely very close to the equilibrium value.

Based on the calculated recovery and wall enthalpies, the calculated heat transfer coefficient using Eq. (17) for a cold wall heat flux of 1×10^7 W/m^2 is between 1 and 2 $kg/(m^2\text{-s})$, as shown in Table 2. However, these calculated values are higher than typical heat transfer coefficients ($\sim 10^{-1}$ $kg/(m^2\text{-s})$). Therefore, it is conceivable that using these coefficients will lead to unrealistic simulation results (see Section 4.4).

4.3. Material system and numerical implementation

In addition to the convective heat transfer coefficient and the recovery enthalpy, the material system, including the thermophysical and transport properties of the PICA samples, the pyrolysis gas properties, as well as the thermochemistry data (B'_g and h_w, note that here the wall enthalpy considers a ablating surface condition, which is different from the one used in the calibration of heat transfer coefficient (see Table 2)), also needs to be provided for the ablation model for PICA. Although the microstructure and ablation behavior of PICA have been studied [48,49], unfortunately, the material model for PICA is not available in the public domain. In this study, the Theoretical Ablative Composite for Open Testing (TACOT) material system is used for the model assessment [36]. Such a material system has also been used in Refs. [27,28] for model validations with PICA samples.

The numerical prediction is then performed using the proposed FEA procedure with ABAQUS (see Fig. 2). The computational domain, mesh configurations, laptop configurations are the same with those used in our prior model verification work [26]. The computational predictions of temperature and ablation histories are discussed and compared with the experimental data in the section below.

4.4. Results for model assessment

4.4.1. Comparison between simulation results and experimental data

Fig. 4 provides a comparison of predictions with the experimental data for the ablation history. Here, the “equilibrium” in the legend denotes the simulation case using the heat transfer coefficient calculated by assuming an equilibrium combustion of acetylene oxygen ($\rho_e U_e C_H = 1.067723$, see Section 4.2), while the “frozen” denotes the case using the heat transfer coefficient calculated by assuming a frozen condition on the surface ($\rho_e U_e C_H = 2.314697$, see Section 4.2). As one can see from Fig. 4, using those heat transfer coefficients, the resulting recession rates are much higher than the experimental data (see also in Table 3). In particular, the reported total ablation depth after the PICA sample had been exposed to the oxy-acetylene torch for 30 s is 7.1 mm, the predictions

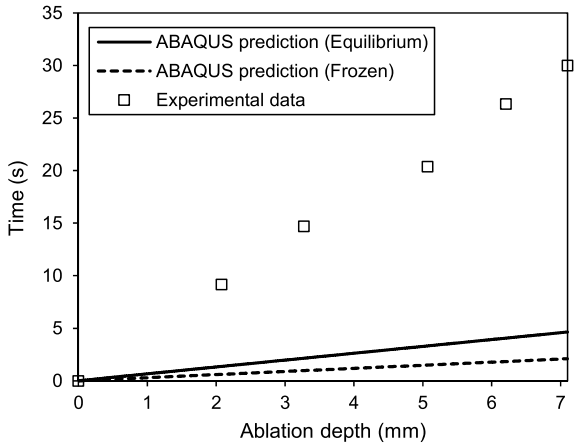

Fig. 4. Comparison of ablation depth predicted using ABAQUS with reported experimental data.

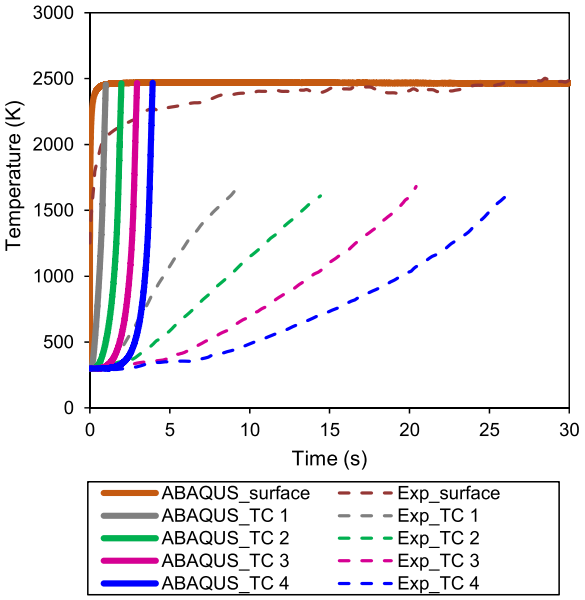

Fig. 5. Comparison of temperature histories on the surface and at four thermocouple locations predicted using ABAQUS (equilibrium case) with experimental data. (For interpretation of the colors in the figure(s), the reader is referred to the web version of this article.)

show, however, the recession reaches the same depth with only 4.64 s (equilibrium) and 2.10 s (frozen). The recession rate is 6.38 times (equilibrium) and 14.08 times (frozen) higher than the experimental data.

A comparison of prediction (equilibrium) and experimental data for the temperature history is illustrated in Fig. 5. It can be seen that although the predicted surface temperature agrees fairly well with the experimental data (after 10 s), the in-depth temperature predictions at four thermocouple locations (i.e., TC_1, TC_2, TC_3, and TC_4) are significantly different from the experimental data.

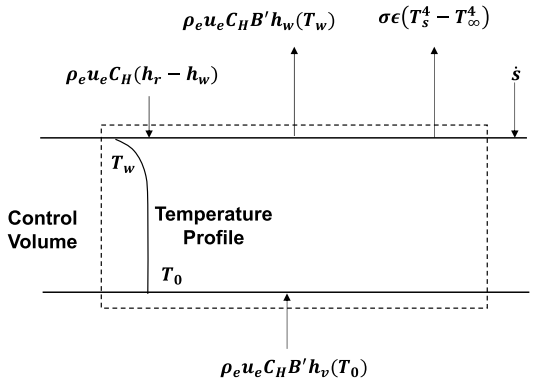

Fig. 6. Energy balance and control volume for steady-state ablation.

Here, the experimental data and the simulation results of the average surface temperature, times when recession reaches 7.1 mm, and the average recession rate are tabulated in Table 3. To investigate possible reasons for the inconsistency between the simulation results and experimental data, a steady-state ablation analysis is performed in the section below to check the effects of the convective heat transfer coefficients on the temperature and ablation responses.

4.4.2. Steady-state ablation analysis of TACOT subjected to an oxy-acetylene torch

When steady-state conditions occur, it is possible to write the energy balance around a control volume extending just above the ablating surface and far down into the material where the temperature has reached ambient material conditions, as shown in Fig. 6.

An energy balance around the control volume shown in Fig. 6 results in the following equation:

$$\rho_e U_e C_H \cdot (h_r - h_w) - \rho_e U_e C_H B' \cdot (h_w - h_v) - \sigma\varepsilon\left(T_w^4 - T_\infty^4\right) = 0, \tag{18}$$

where the terms in Eq. (18) represent in order from left to right: convective flux, energy due to mass removal (h_v is the enthalpy of the virgin solid at room temperature), and re-radiation. Note that the energy balance is independent of the specific heat transfer and decomposition processes occurring within the material. The total mass loss rate is composed of the in-depth pyrolysis mass flux $\dot{m}_g$ and the surface char flux $\dot{m}_c$, but only the total mass flux needs to be determined and the knowledge of the values of the individual fluxes is not needed in the energy balance.

Solution for the steady-state temperature and mass loss is obtained by solving the overall energy balance in Eq. (18) in conjunction with the surface thermochemical relationship Eqs. (13)-(15). Finally, since steady-state conditions occur, the ratio of the char to pyrolysis mass flux can be expressed as:

$$\frac{B_c'}{B_g'} = B_{ss}, \tag{19}$$

where B_{ss} is a constant based on the decomposition characteristics of the constituent components of the composite and is computed from the virgin and char densities.

Table 3
Comparison between numerical predictions and experimental data.

Parameter	Experimental	ABAQUS Prediction (using $\rho_e U_e C_H$ calculated for the equilibrium case)	ABAQUS Prediction (using $\rho_e U_e C_H$ calculated for the frozen case)
Avg. surface temperature (K)	2400	2450	2680
Time to reach 7.1 mm recession (s)	30.00	4.64	2.10
Avg. recession rate (mm/s)	0.24	1.53	3.38

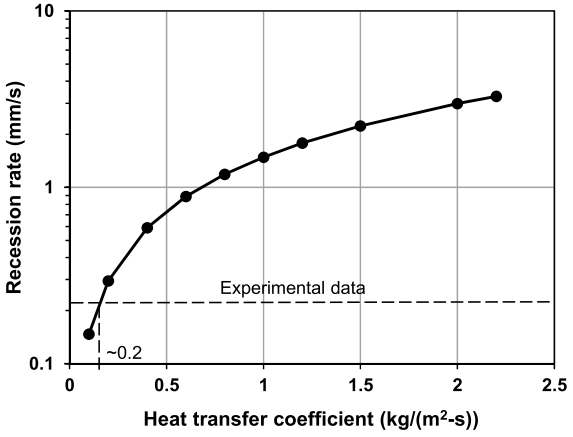

Fig. 7. Recession rate versus heat transfer coefficient for steady-state ablation of TACOT subjected to the oxy-acetylene torch flame.

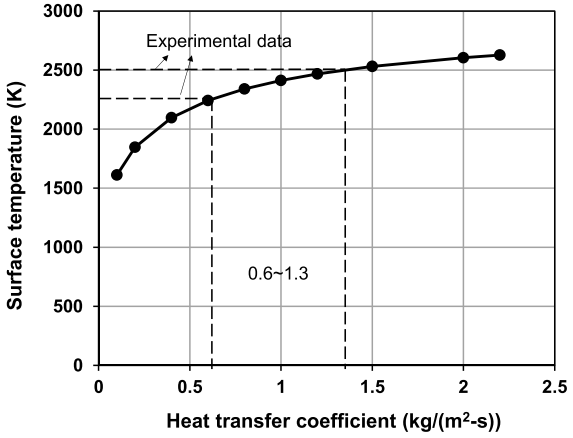

Fig. 8. Surface temperature versus heat transfer coefficient for steady-state ablation of TACOT subjected to the oxy-acetylene torch flame.

At the steady state, the ratio of char to pyrolysis mass loss is a fixed value given by the composition of the base material. For the TACOT material, the virgin density is 280 kg/m^3 and the char density is 220 kg/m^3. Therefore, the pyrolysis loss is 60 kg/m^3, and the ratio of char to pyrolysis mass loss is 3.666 (i.e., 220/60), so that the final constraint becomes:

$$\frac{B'_c}{B'_g} = 3.666, \tag{20}$$

For TACOT, $h_v = -857$ J/g and for the acetylene torch conditions $h_r = 1693$ J/g. The emissivity ε is assumed to be 0.9. Recession rates and surface temperatures for various values of the heat transfer coefficient are shown in Figs. 7 and 8. Note also the range of the experimental data is also shown.

The results show that there is not one single value for the heat transfer coefficient that matches both the measured recession rate and surface temperature. In other words, the recession and surface temperature torch data together are not consistent with the TACOT model. To the authors' knowledge, there could be four possibilities for causing such an inconsistency: (i) the TACOT model used in the simulation doesn't represent the true material property of PICA well, (ii) The thermocouple wires used in the experimental test were too thick, which removed the heat from the junction and resulted in low measured temperatures, (iii) The torch and sample were too small, and do not represent a 1-D configuration, and (iv) The surface kinetics may be finite and the assumption of equilibrium at the surface (see Section 4.2) was not valid.

5. Conclusion

In this paper, an FEA has been performed with ABAQUS for a 1-D charring ablation model to predict the temperature and ablation histories of a PICA sample subjected to oxy-acetylene torch flame. Multiple ABAQUS subroutines have been developed to account for the effects of material decomposition, charring, and progressive material removal in the heat transfer governing equation and the surface energy balance yielded boundary conditions. The recovery enthalpy and the convective heat transfer coefficient for the ablation model have been calculated based on the gas compositions and two assumed surface conditions (i.e., equilibrium and frozen). Using the calculated recovery enthalpy and the convective heat transfer coefficient, the predicted surface temperature showed fair agreement with the experimental data. However, the predicted recession rate was 6.38 times (equilibrium) and 14.08 times (frozen) higher than the experimental data. To investigate such an inconsistency, a steady-state ablation analysis has been proposed to check the effect of the heat transfer coefficient on the surface temperature and recession rate. Results of the steady-state ablation analysis indicate that there was no single value for the heat transfer coefficient to match both the surface temperature and recession rate. Possible reasons for such an inconsistency include: (i) TACOT model doesn't represent PICA well, (ii) Thermocouple wires were too thick removing heat from the junction and resulting in low measured temperatures, (iii) The torch and sample were too small not representing a 1-D configuration, and (iv) Surface kinetics may be finite and the assumption of equilibrium at the surface was not valid. Despite the inconsistency between the current predictions and the experimental data, this paper provides a semi-empirical procedure for approximating the surface boundary conditions for the oxy-acetylene torch test platform based on the traditional hypersonic flow approaches as well as a preliminary method for the evaluation of the inconsistency based on a steady-state ablation analysis. The current validation attempt is also of great significance for the future model validation effort on the charring ablation because it provides useful recommendations on (i) the potential directions to improve the accuracy of temperature measurement for future ablation test designs and (ii) potential directions to improve the representativeness and accuracy of the future charring ablation models for PICA. In the future, a more rigorous model needs to be developed based on the aero thermal computational fluid dynamics (CFD) to investigate the torch environment and validate the traditional hypersonic flow approaches through comparisons with experimental diagnostics.

Declaration of Competing Interest

The authors have no competing interest to declare.

Acknowledgements

This work was supported by the Air Force Research Laboratory (AFRL) under contract no. FA8651-08-D-0108 and task order no. 42. Any opinions, findings, conclusions, or recommendations expressed in this work are those of the authors and do not necessarily reflect the views of the AFRL. Y. Wang also thanks Dr. Crystal L. Pasiliao (AFRL/RW) and Prof. David W. Hahn (University of Florida) for their support in this research.

References

[1] J.D. Anderson, Hypersonic and High Temperature Gas Dynamics, AIAA, 2000.
[2] H.K. Tran, C. Johnson, D. Rasky, F. Hui, M.T. Hsu, T. Chen, Y.K. Chen, D. Paragas, L. Kobayashi, Phenolic Impregnated Carbon Ablators PICA as Thermal Protection System for Discovery Missions, NASA TM-110440, NASA, Washington, DC, 1997.

[3] M. Natali, J.M. Kenny, L. Torre, Science and technology of polymeric ablative materials for thermal protection systems and propulsion devices: a review, Prog. Mater. Sci. 84 (2016) 192–275.
[4] J.A. Dec, Three dimensional finite element ablative thermal response analysis applied to heatshield penetration design, PhD Thesis, Georgia Institute of Technology, 2010.
[5] E.P. Bartlett, R.M. Kendall, R.A. Rindal, A multicomponent boundary layer chemically coupled to an ablating surface, AIAA J. 5 (1967) 1063–1071.
[6] Y.K. Chen, F.S. Milos, Ablation and thermal response program for spacecraft heatshield analysis, J. Spacecr. Rockets 36 (1999) 475–483.
[7] Y.K. Chen, F.S. Milos, Two-dimensional implicit thermal response and ablation program for charring materials, J. Spacecr. Rockets 38 (2001) 473–481.
[8] Y.K. Chen, F.S. Milos, Multidimensional finite volume fully implicit ablation and thermal response code, J. Spacecr. Rockets 55 (2018) 914–927.
[9] J. Lachaud, T.E. Magin, I. Cozmuta, N.N. Mansour, A short review of ablative-material response models and simulation tools, in: 7th Aerothermodynamics Symposium, Bruggw, Belgium, 2011.
[10] D.W. Kuntz, B. Hassan, D.L. Potter, Predictions of ablating hypersonic vehicles using an iterative coupled fluid/thermal approach, J. Thermophys. Heat Transf. 15 (2001) 129–139.
[11] H. Weng, A. Martin, Multidimensional modeling of pyrolysis gas transport inside charring ablative materials, J. Thermophys. Heat Transf. 28 (2014) 583–597.
[12] E.D. Farbar, H. Alkandry, J. Wiebenga, I.D. Boyd, Simulation of ablating hypersonic vehicles with finite-rate surface chemistry, in: 11th AIAA/ASME Joint Thermophysics and Heat Transfer Conference, 2014, p. 2124.
[13] J. Lachaud, N.N. Mansour, Porous-material analysis toolbox based on OpenFOAM and applications, J. Thermophys. Heat Transf. 28 (2014) 191–202.
[14] J.B.E. Meurisse, J. Lachaud, F. Panerai, C. Tang, N.N. Mansour, Multidimensional material response simulations of a full-scale tiled ablative heatshield, Aerosp. Sci. Technol. 76 (2018) 497–511.
[15] W. Li, H. Huang, Y. Tian, Z. Zhao, Nonlinear analysis on thermal behavior of charring materials with surface ablation, Int. J. Heat Mass Transf. 84 (2015) 245–252.
[16] W. Li, H. Huang, B. Ai, Z. Zhang, On the novel designs of charring composites for thermal protection application in reentry vehicles, Appl. Therm. Eng. 93 (2016) 849–855.
[17] W. Li, H. Huang, X. Xu, A coupled thermal/fluid/chemical/ablation method on surface ablation of charring composites, Int. J. Heat Mass Transf. 109 (2017) 725–736.
[18] S. Shi, L. Li, J. Liang, S. Tang, Surface and volumetric ablation behaviors of SiFRP composites at high heating rates for thermal protection applications, Int. J. Heat Mass Transf. 102 (2016) 1190–1198.
[19] J. Scoggins, N. Mansour, H. Hassan, Development of reduced kinetic mechanism for PICA pyrolysis products, in: 42nd AIAA Thermophysics Conference, American Institute of Aeronautics and Astronautics, 2011.
[20] J. Lachaud, T. van Eekelen, J.B. Scoggins, T.E. Magin, N.N. Mansour, Detailed chemical equilibrium model for porous ablative materials, Int. J. Heat Mass Transf. 90 (2015) 1034–1045.
[21] J.A. Dec, R.D. Braun, Three-dimensional finite element ablative thermal response and design of thermal protection systems, J. Spacecr. Rockets 50 (2013) 725–734.
[22] J.A. Dec, R.D. Braun, B. Lamb, Ablative thermal response analysis using the finite element method, J. Thermophys. Heat Transf. (2012) 201–212.
[23] T.K. Risch, Verification of a finite-element model for pyrolyzing ablative materials, in: 47th AIAA Thermophysics Conference, Denver, USA, 2017, p. 3354.
[24] A.J. Amar, B. Oliver, B. Kirk, G. Salazar, J. Droba, Overview of the CHarring Ablator Response (CHAR) code, in: 46th AIAA Thermophysics Conference, AIAA AVIATION Forum, 2016, p. 3385.
[25] M.E. Ewing, B. Pincock, Heat transfer modeling of a charring material using isoconversional kinetics, Heat Transf. Eng. 38 (2017) 1189–1197.
[26] Y. Wang, T.K. Risch, C.L. Pasiliao, Modeling of pyrolyzing ablation problem with ABAQUS: a one-dimensional test case, J. Thermophys. Heat Transf. 32 (2017) 544–546.
[27] J.H. Langston, F. Stefani, M. Salita, J.H. Koo, Validation of ablative material response model using charring ablator response program, in: SAMPE 2017 ISTC, Seattle, WA, 2017.
[28] J.H. Langston, C. Wong, N. Diaz, F. Stefani, J.H. Koo, M. Salita, Validation of ablation model of PICA using fully implicit ablation and thermal response program, in: 55th AIAA Aerospace Sciences Meeting, Grapevine, Texas, 2017, p. 0896.
[29] P. Schrooyen, A. Turchi, K. Hillewaert, P. Chatelain, T.E. Magin, Two-way coupled simulations of stagnation-point ablation with transient material response, Int. J. Therm. Sci. 134 (2018) 639–652.
[30] A. Martin, I.D. Boyd, Strongly coupled computation of material response and nonequilibrium flow for hypersonic ablation, J. Spacecr. Rockets 52 (2014) 89–104.
[31] M. Natali, I. Puri, M. Rallini, J. Kenny, L. Torre, Ablation modeling of state of the art EPDM based elastomeric heat shielding materials for solid rocket motors, Comput. Mater. Sci. 111 (2016) 460–480.
[32] A. Harpale, S. Sawant, R. Kumar, D. Levin, H.B. Chew, Ablative thermal protection systems: pyrolysis modeling by scale-bridging molecular dynamics, Carbon 130 (2018) 315–324.
[33] G. Duffa, Ablative Thermal Protection Systems Modeling, American Institute of Aeronautics and Astronautics, Inc., 2013.
[34] A. Turchi, D. Bianchi, F. Nasuti, M. Onofri, A numerical approach for the study of the gas-surface interaction in carbon-phenolic solid rocket nozzles, Aerosp. Sci. Technol. 27 (2013) 25–31.
[35] Test Case Baseline Results, in: T. Risch, C. Kostyk (Eds.), 5th Ablation Workshop, Ablation Test-Case Series, vol. 2, 2012, https://uknowledge.uky.edu/cgi/viewcontent.cgi?article=1049&context=ablation.
[36] T. van Eekelen, A. Martin, J. Lachaud, D. Bianchi, in: 6th Ablation Workshop, in: Ablation Test Case Series, vol. 3, University of Illinois, 2014.
[37] C.A. Snyder, Chemical Equilibrium with Applications, NASA Glenn Research Center, 2016, https://www.grc.nasa.gov/www/CEAWeb/.
[38] ABAQUS User Subroutine Reference Manual, ABAQUS 6.14 Documentation.
[39] Y. Wang, Multiphysics analysis of lightning strike damage in laminated carbon/glass fiber reinforced polymer matrix composite materials: a review of problem formulation and computational modeling, Composites, Part A, Appl. Sci. Manuf. 101 (2017) 543–553.
[40] Y. Wang, C.L. Pasiliao, Modeling ablation of laminated composites: a novel manual mesh moving finite element analysis procedure with ABAQUS, Int. J. Heat Mass Transf. 116 (2018) 306–313.
[41] Y. Wang, N. Shen, G.K. Befekadu, C.L. Pasiliao, Modeling pulsed laser ablation of aluminum with finite element analysis considering material moving front, Int. J. Heat Mass Transf. 113 (2017) 1246–1253.
[42] S. Gordan, B.J. McBride, Chemical Equilibrium with Applications, NASA Glenn Research Center, 2017.
[43] J.A. Fay, F.R. Riddell, Theory of stagnation point heat transfer in dissociated air, J. Aeronaut. Sci. 25 (1958) 73–85.
[44] M. Salita, Addition to the NASA_Lewis Thermochemical Program of Afterburning and Flowfield Calculations for Mixing Plumes, Thioko Report 2814-83-M125, 1983.
[45] NIST, Chemistry WebBook, SRD 69, 2018.
[46] C.A. Powars, R.M. Kendall, User's Manual Aerotherm Chemical Equilibrium (ACE) Computer Program, NASA, 1972.
[47] B.J. McBride, S. Gordon, Computer Program for Calculation of Complex Chemical Equilibrium Compositions and Applications II. Users Manual and Program Description. 2; Users Manual and Program Description, NASA Lewis Research Center, 1996.
[48] M. Natali, I. Puri, J.M. Kenny, L. Torre, M. Rallini, Microstructure and ablation behavior of an affordable and reliable nanostructured Phenolic Impregnated Carbon Ablator (PICA), Polym. Degrad. Stab. 141 (2017) 84–96.
[49] B. Helber, A. Turchi, J.B. Scoggins, A. Hubin, T.E. Magin, Experimental investigation of ablation and pyrolysis processes of carbon-phenolic ablators in atmospheric entry plasmas, Int. J. Heat Mass Transf. 100 (2016) 810–824.